Tellus (2006), 58B, 537–549
Printed in Singapore. All rights reserved

TELLUS

Simulating dynamics of $-^{13}C$ of CO_2 in the planetary boundary layer over a boreal forest region: covariation between surface fluxes and atmospheric mixing

By BAOZHANG CHEN[1]*, JING M. CHEN[1], PIETER P. TANS[2] and LIN HUANG[3]; [1]*Department of Geography and Program in Planning, University of Toronto, 100 St. George Street, Room 5047, Toronto, ON M5S 3G3, Canada;* [2]*National Oceanic and Atmospheric Administration/Earth System Research Laboratory, Climate Monitoring Division, 325 Broadway, Boulder, CO 80305, USA;* [3]*Atmospheric Science and Technology Directorate, Science & Technology Branch, Environment Canada, 4905 Dufferin Street, Toronto, ON M3H 5T4, Canada*

(Manuscript received 14 Jannuary 2006; in final form 30 June 2006)

ABSTRACT

Stable isotopes of CO_2 contain unique information on the biological and physical processes that exchange CO_2 between terrestrial ecosystems and the atmosphere. Ecosystem exchange of carbon isotopes with the atmosphere is correlated diurnally and seasonally with the planetary boundary layer (PBL) dynamics. The strength of this kind of covariation affects the vertical gradient of $\delta^{13}C$ and thus the global $\delta^{13}C$ distribution pattern. We need to understand the various processes involved in transport/diffusion of carbon isotope ratio in the PBL and between the PBL and the biosphere and the troposphere. In this study, we employ a one-dimensional vertical diffusion/transport atmospheric model (VDS), coupled to an ecosystem isotope model (BEPS-EASS) to simulate dynamics of $^{13}CO_2$ in the PBL over a boreal forest region in the vicinity of the Fraserdale (FRD) tower (49°52′29.9″N, 81°34′12.3″W) in northern Ontario, Canada. The data from intensive campaigns during the growing season in 1999 at this site are used for model validation in the surface layer. The model performance, overall, is satisfactory in simulating the measured data over the whole course of the growing season. We examine the interaction of the biosphere and the atmosphere through the PBL with respect to $\delta^{13}C$ on diurnal and seasonal scales. The simulated annual mean vertical gradient of $\delta^{13}C$ in the PBL in the vicinity of the FRD tower was about 0.25‰ in 1999. The $\delta^{13}C$ vertical gradient exhibited strong diurnal (29%) and seasonal (71%) variations that do not exactly mimic those of CO_2. Most of the vertical gradient (96.5% ±) resulted from covariation between ecosystem exchange of carbon isotopes and the PBL dynamics, while the rest (3.5%±) was contributed by isotopic disequilibrium between respiration and photosynthesis. This disequilibrium effect on $\delta^{13}C$ of CO_2 dynamics in PBL, moreover, was confined to the near surface layers (less than 350 m).

1. Introduction

One of the crucial issues in the prognoses of future climate change is the global budget of atmospheric CO_2. To investigate the current and historical global carbon budgets and to predict the future tends in atmospheric CO_2, it is critical to determine the spatial and temporal patterns of carbon sources and sinks and to understand the mechanisms for natural carbon sequestration (Enting et al., 1995). One of most often used approaches for this purpose in recent years has been to conduct inversions of atmospheric CO_2 measurements and related isotopes.

Inversion calculations exploit the atmospheric CO_2 measurements through the use of atmospheric transport models, which in theory should provide a causative direct connection between the distribution of the surface sources and sinks and observations at the CO_2 monitoring stations. A summary of the results of a model comparison exercise called TransCom3 involving 16 atmospheric transport models from various research groups indicates that the uncertainty in the estimates of magnitude and distribution of the surface sinks/sources is considerable (Gurney et al., 2002), which is one of the largest concerns in the inverse calculation. In order to reduce the uncertainty in net CO_2 flux estimate, various problems such as uniqueness of a model solution that depends on observing density and the resolution of the model source function have to be solved properly. Additionally, the inversion methodology faces problems related to covariation between atmospheric mixing and surface fluxes, which has been

* Corresponding author.
e-mail: chenb@geog.utoronto.ca
DOI: 10.1111/j.1600-0889.2006.00213.x

called the 'atmospheric CO_2 rectifier' effect by Denning et al. (1996a, b). This effect is defined as a spatial concentration gradient of a specified trace gas in the atmosphere, averaged over a certain time interval, caused by surface fluxes that are varying in time but have zero mean when averaged over that same time interval. The gradient results from the covariation between the surface flux and atmospheric transport on many space and time scales, from synoptic to global and from daily to annual. The broad definition of the rectifier effect includes both vertical and horizontal (terrestrial and marine-land) rectifiers of CO_2, CO, O_2 and other tracers at any temporal scale (seasonal and diurnal) (Pearman and Hyson, 1980; Denning et al., 1995, 1996a,b, 1999; Stephens et al., 1998; Stephens 1999; Chen et al., 2004), and also includes the isotope-ratio rectifiers corresponding to these terrestrial—concentration effects (Stephens et al., 2000). Transport models have of course incorporated such effects implicitly, but unless we understand the details of the mechanisms of this covariation, it can lead to wrong estimates of the surface fluxes from inverting the background CO_2 measurements (Denning et al., 1999, Chan B. et al., 2004).

The stable isotope ratio of carbon dioxide (δ^{13}C) in the atmosphere contains unique information to study the overall balance of surface CO_2 fluxes (Tans, 1980, 1993). Atmospheric inversion using CO_2 concentration data, complemented with δ^{13}C data, has produced meaningful results for the global carbon budget and its temporal dynamics (Ciais et al., 1995a,b; Denning et al., 1995; Enting et al., 1995; Fan et al., 1998; Gurney et al., 2002). It is recognized that the atmospheric measurements are still too sparse, relative to its spatial variability, to be used for inferring the surface flux at high spatial resolution (Ciais et al., 1995a). The use of the isotope ratio as an additional constraint to identify various carbon sources and sinks can contribute to a significant reduction in the uncertainty. Similar to using CO_2 concentration data, the inversion methodology using δ^{13}C of CO_2 also faces problems related to the rectification effect. Unless we understand the details of the mechanisms of the covariation between the surface isotope flux and atmospheric transport, it will also lead to a largely biased estimate of the surface fluxes from inverting the background δ^{13}C measurements. Therefore, it is crucial to estimate the strength of isotope rectification and to understand its mechanism for inversion modelling using δ^{13}C data.

The isotope rectification occurs mostly due to the control of planetary boundary layer (PBL) on the vertical transport of heat and mass. We need to understand the various processes involved in transport of the carbon isotope ratio in the PBL, between the PBL and the biosphere, and between the PBL and the troposphere.

In this study, we address part of this issue by elucidating some aspects of the vertical rectifier effect over a boreal forest region through demonstrating the impacts of diurnal and seasonal atmospheric processes (i.e. the PBL dynamics) on a regional vertical distribution of carbon isotope ratio. We emphasize the importance of the interaction between the PBL dynamics and the biospheric isotope flux (isoflux), and that uncoupling the atmosphere and the land biosphere with respect to δ^{13}C of CO_2 (as in global inversion models with a neutral surface flux density) could lead to a biased estimate of the land surface CO_2 and carbon isofluxes.

We employ a one-dimensional vertical transport atmospheric model (VDS) (Chen et al., 2004, 2005a), coupled to an ecosystem isotope model (BEPS-EASS) (Chen et al., 2006) to simulate dynamics of ^{13}C of CO_2 in the PBL over a boreal forest region in the vicinity of the Fraserdale (FRD) tower in northern Ontario, Canada. After verification of the coupled model, we examine the interaction of the biosphere and the atmosphere with respect to δ^{13}C, as well as the atmospheric mixing processes on diurnal and seasonal scales in 1999. Then we investigate the carbon isotope rectifier effect over this region as an example. In addition, we perform model experiments, in which the isofluxes derived by the BEPS-EASS isotope model is prescribed without a diurnal cycle (e.g. using daily mean value) or is calculated using daily overall carbon isotopic signature of net CO_2 flux (i.e. presume the respired and photosynthetic fluxes have the same isotopic signatures) to investigate the impact of the diurnal cycle on the carbon isotope rectifier effect or the effect of disequilibrium of isotopic fractionation on dynamics of ^{13}C of CO_2 in the PBL.

2. Methodology

In order to account for the influences of turbulent mixing in the convective boundary layer (CBL) and entrainment of the air aloft on diffusion and on the estimates of $^{13}CO_2$ discrimination, we designed a one-dimensional ecosystem–boundary layer isotope model (VDS–BEPS-EASS) (Chen et al., 2006) based on isotopic mass conservation and energy balance, which involves the interaction between plant canopies and the atmosphere in the surface layer (i.e. ^{13}C discrimination) and $^{13}CO_2$ diffusion through the PBL, using remotely sensed surface parameters to characterize the surface heterogeneity.

The lowest layer in this model is set at a fixed height of 20 m. The levels above are separated by intervals of 50 m in the model domain (2520 m; see fig. 2 in Chen et al., 2004). The computing time step is 30 s. Since the gradients of CO_2 and $^{13}CO_2$ are usually strong in the lower surface layers at nighttime, especially under fair weather conditions when temperature inversion is great. The fixed 50 m vertical resolution in the model might not be sufficient. We are currently updating the VDS model with higher spatial resolution (i.e. 20 m interval). There are different schemes in the model to treat the stable/nocturnal and the free-convection PBL structures (Chen et al., 2005a). The criteria that determine which module is applicable are the sign and magnitude of the bulk Richardson number (R_b) in the surface layer, and the magnitude of the ratio of the CBL height to the Monin Obukhov length ($|z_h/L|$) (Chen et al., 2005a).

The sensible heat flux on top of the model domain (above 2.5 km from the ground, usually above CBL) is set to zero throughout the year. However, as one-dimensional model boundary conditions, it is critical to determine the time-dependent CO_2 and $\delta^{13}C$ of CO_2 at the top of CBL. The Globalview reference marine boundary layer (MBL) data for CO_2 and $\delta^{13}C$ (Masarie and Tans, 1995; Globalview-CO_2, 2005) are used as model top boundary conditions. We use a linear interpolation method to extract these values at the same latitude and time as the study site. The technique making use of both the 24-h minima tower measurements and the Globalview reference MBL matrix data (Chen et al., 2004) is introduced for CO_2 top condition calculation, whereas MBL-$\delta^{13}C$ data are approximately used as its top condition since the $\delta^{13}C$ values correspondent to the 24-h minima tower measurements are not available (Chen et al., 2006).

The model bottom conditions are the fluxes of sensible heat, carbon and isotopic $^{13}CO_2$ in the surface layer (the bottom layer of the model domain, i.e. 20 m height), which are modelled from the expanded BEPS-EASS isotope model (Chen et al., 2006).

The net ecosystem exchange ($F_{net,C}$) of CO_2 (with the atmospheric convention, upwards positive and in μmol m^{-2} s^{-1}) at the interface between terrestrial ecosystems and the atmosphere is calculated using eq. (1),

$$F_{net,C} = F_A + F_R, \tag{1}$$

where F_A is the carbon uptake during daytime by photosynthesis (gross primary production) and F_R is the carbon loss by respiration (total ecosystem respiration). Correspondingly, the isoflux ($F_{\delta 13}$, in μmol m^{-2} s^{-1} ‰) can be expressed as,

$$F_{\delta 13} = \delta^{13}C_{bio} F_{net,C} = \delta^{13}C_A F_A + \delta^{13}C_R F_R, \tag{2}$$

where $\delta^{13}C_{bio}$,$\delta^{13}C_A$ and $\delta^{13}C_R$ are the flux weighted stable carbon isotopic signatures of net CO_2 flux, of gross primary production flux, of ecosystem respiration flux, and in per mil (‰). $\delta^{13}C_A$is the difference between the isotopic signature of ambient CO_2 in the canopy ($\delta^{13}C_a$) and the whole-canopy integrated photosynthetic carbon isotope discrimination (Δ_{canopy}), i.e. $\delta^{13}C_A = \delta^{13}\,C_a - \Delta_{canopy}$. The Δ_{canopy} is calculated as the flux-weighted average of net carbon assimilation for sunlit leaves and shaded leaves (Chen et al., 2006). The photosynthetic discrimination against $^{13}CO_2$ at the leaf level (Δ, in per mil, ‰) is computed according to previous methods (Farquhar et al., 1989; Farquhar and Lloyd, 1993; Lloyd et al., 1996).

The coupled ecosystem–boundary layer isotope model is forced by the near-surface hourly meteorological variables (i.e. at 20 m height in this study), including air temperature (T_a), air relative humidity (RH), in-coming shortwave radiation (RAD), wind speed (u) and precipitation (P). The land surface data, including vegetation and soil data are also needed as model inputs. Most of vegetation parameters, such as land cover type (LC), leaf area index (LAI) and foliage clumping index (Ω) are derived from satellite images instead of directly using observed canopy data. LC and LAI are derived from satellite images at 1 km resolution (directly from AVHRR images, or up-scaling from Landsat TM) (Cihlar et al., 1999; Chen et al., 2002); while Ω is approached using multiangular POLDER 1 data on a methodology documented by Chen et al. (2005) and Leblanc et al. (2005) which significantly alters sunlit and shaded leaf separation, canopy radiation environment and therefore affects water, heat, carbon as well as photosynthesis discrimination. Soil properties are obtained from SLC database version 1.0 and 2.0 (Tarnocai, 1996; Lacelle, 1998).

The FRD tower is taken as an experiment site, which is located southwest of James Bay in northern Ontario, Canada (49°52′29.9″N, 81°34′12.3″W; 210 m above sea level). According to a Landsat TM image at a 30 m resolution (2000), the landscape (3600 km^2 around the tower) consists of 66% of black spruce (*Picea mariana*) and Jack pine (*Pinus banksiana*), 20% open land after forest fires and logging, 11% aspen (*Populus tremuloides*) and paper birch (*Betula papyrifera*), and 3% open water. The overstorey vegetation heights around this site are ranging from 10 to 15 m.

Most of the hourly meteorological variables as model inputs are available for the FRD tower. T_a is measured at four levels (1.5, 10, 20 and 40 m) while RH and u are taken at three levels (1.5, 20 and 40 m; and 10, 20 and 40 m, respectively). The multi-layers measurements provide a greater temporal coverage than would otherwise be possible, gaps with no valid data at any level are less than 10%. In this study, small data gaps of 1–2 h are filled by linear interpolation. When missing data are longer than 3 h, the spatial interpolation method is used. Unfortunately, precipitation is not measured for the FRD tower. We approximately use the precipitation data measured at the weather station Kapuskasing (87 km southwest of FRD) as a proxy. RAD is only observed at one level (i.e. 40 m). Gaps of durations $\geq$ 3 h (up to 2 weeks) for RAD are filled by a solar irradiance model based on Bristow–Campbell algorithms, in which the total daily solar irradiance (R_s) is calculated from the limited data set of daily maximum and minimum air temperature and daily total precipitation, along with site latitude, elevation, and annual mean temperature (Bristow and Campbell, 1984; Winslow et al., 2001) (see appendix A in Chen et al., 2005a for more details).

Atmospheric CO_2 concentration is measured at 20 and 40 m heights on FRD tower, according to the WMO (Global Atmospheric Watch) guidelines, with an accuracy of 0.1 ppm (Higuchi et al., 2003). Three intensive campaigns for flask-air sampling (at 20 m height) collected in the growing season of 1999 (early growing season: 2–7 June; middle growing season: 21–23 July; and late growing season: 10–10 September) at this site are used for the model validation in the surface layer. Each campaign lasted for 3–6 d, with a sampling frequency of 2 h. Air samples were taken in 2 L flasks at the 20 m level of the tower. The flasks were pressurized up to 15 PSI above ambient pressure and were dried cryogenically (−70°C) to remove water vapour. The isotopic measurements were directly traced back to the primary standard VPDB through two-carbonate-linkages (i.e. lab

running standards) (Huang et al., 2003). The assigned ratio for the primary standard (VPDB CO_2) is 0.0112372 for carbon. The accuracy and precision (including vacuum extraction and IRMS measurements) is 0.02‰ for $\delta^{13}C$ (Huang et al., 2003).

3. Vertical profiles of $-^{13}C$ of CO_2

3.1. Diurnal vertical profiles

The computed isotopic compositions (i.e. $\delta^{13}C$ values) at the surface layer (i.e. at 20 m height) during the growing season in 1999 at FRD agree well with intensive campaign data. For the three campaign periods (which occurred in early, middle and late growing season, respectively), the squared correlation coefficients (r^2) at hourly time steps are 0.93, 0.76 and 0.71, and the root mean squared error (RMSE) values equal to 0.13‰, 0.34‰ and 0.39‰, respectively. The model performance, overall, is satisfactory in simulating the diurnal variation of $\delta^{13}C$ at 20 m height over the whole course of the growing season.

We select 3 days, a fair weather day (4 June), a cloudy day (23 July) and a rainy day (12 September), to illustrate the simulated vertical diurnal profiles for different phases of the growing season and under varied weather conditions.

During the night preceding 4 June, there existed a very stable air condition with a shallow nocturnal boundary layer (NBL: within 170 m) formed by radiative cooling, a large temperature inversion, a high Richardson number R_i (about 0.15–0.25), and a low friction velocity μ_*. As shown in Fig. 1, both simulated and observed carbon isotope ratios were depleted (more negative) in the surface layer at this night. The stable and shallow NBL trapped the nighttime respired CO_2 with depleted $\delta^{13}C$ near the surface and built up a large nighttime negative peak in $\delta^{13}C$ around sunrise. In contrast, residual (of the previous day PBL) air with enriched (less negative) $\delta^{13}C$ was present above the NBL. This led to a very large gradient in $\delta^{13}C$ of about 1.7‰–2‰ near the surface. The negative peak of $\delta^{13}C$ in the surface layer disappeared rapidly in the morning with the onset of photosynthesis and the breakdown of the surface inversion layer. $\delta^{13}C$ increased from the early morning to midday and the maxima occurred in the afternoon when the mixed layer grew to about 1 km. Through the whole CBL, there was <0.1‰ vertical difference (Fig. 1a) throughout the afternoon. During daytime, $\delta^{13}C$ of CO_2 at the canopy top (i.e. at 20 m) was consistently higher than that above the canopy (>70 m; Fig. 1b), indicating a strong drawdown of forest $^{12}CO_2$ in the canopy top layer due to the expected effects of photosynthetic discrimination against $^{13}CO_2$. After sunset, a new NBL developed, and $\delta^{13}C$ once again began to decrease as photosynthesis gave way to respiration, and $\delta^{13}C$ became more depleted closer to the canopy.

The vertical mixing patterns in $\delta^{13}C$ on 23 July, as a typical cloudy weather condition, are shown in Fig. 2. The NBL was deeper with a smaller temperature inversion while the CBL was shallower with weaker mixing strength on 23 July than on 4 June.

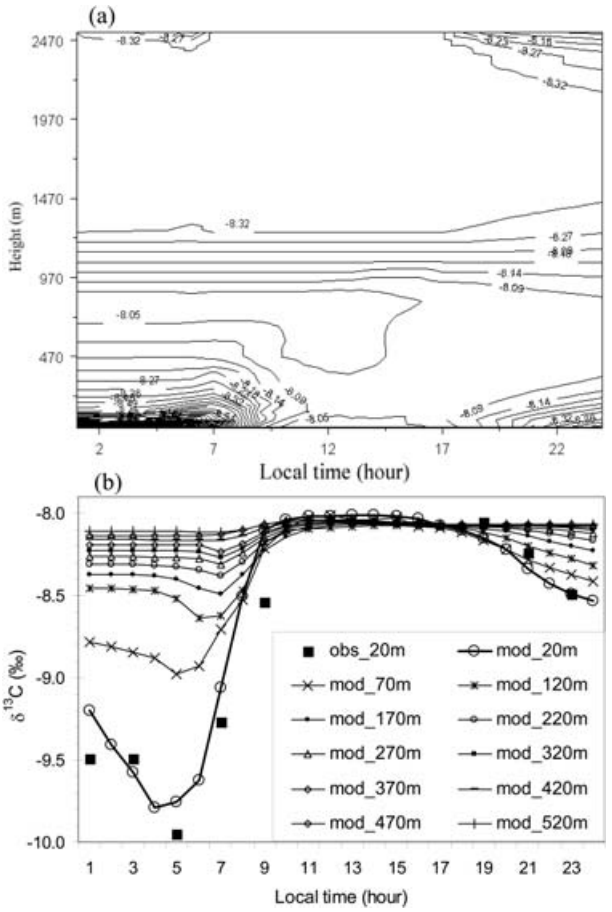

Fig. 1. Time–height cross-section of simulated (multiple heights) and observed (20 m) diurnal variations of $\delta^{13}C$ of CO_2 on 4 June 1999. (a) Two-dimensional contour graph for $\delta^{13}C$ (unit: ‰); (b) vertical profile of diurnal cycles of $\delta^{13}C$ (up to 520 m, obs- campaign measured, mod-simulated).

As a result, the vertical gradient in $\delta^{13}C$ of CO_2 during nighttime was smaller (1.2‰ versus 1.8‰) while it was greater (0.25‰ versus 0.1‰) in the daytime on 23 July.

It was rainy on 12 September, and there was a very weak temperature inversion as well as a very weak vertical mixing strength. The concentration gradient diffusion process of $^{13}CO_2$ was dominant and with a large value of the eddy-transfer coefficient K. The surface signatures of $^{13}CO_2$ diffused to about 400 m at nighttime and around 700 m at daytime (Fig. 3). $\delta^{13}C$ of CO_2 gradually increased with height through the night to early morning, while $\delta^{13}C$ of CO_2 gradually decreased with height through the midday to the afternoon. There was a large inverse vertical gradient of $\delta^{13}C$ (up to 700 m, about 0.5‰) during the afternoon, indicating the weakness in mixing and the photosynthetic discrimination occurring in the canopy top layer.

The model results compared well with the day-to-day variability of the diurnal cycle at the canopy top layer (i.e. 20 m above the ground) under different weather conditions and in

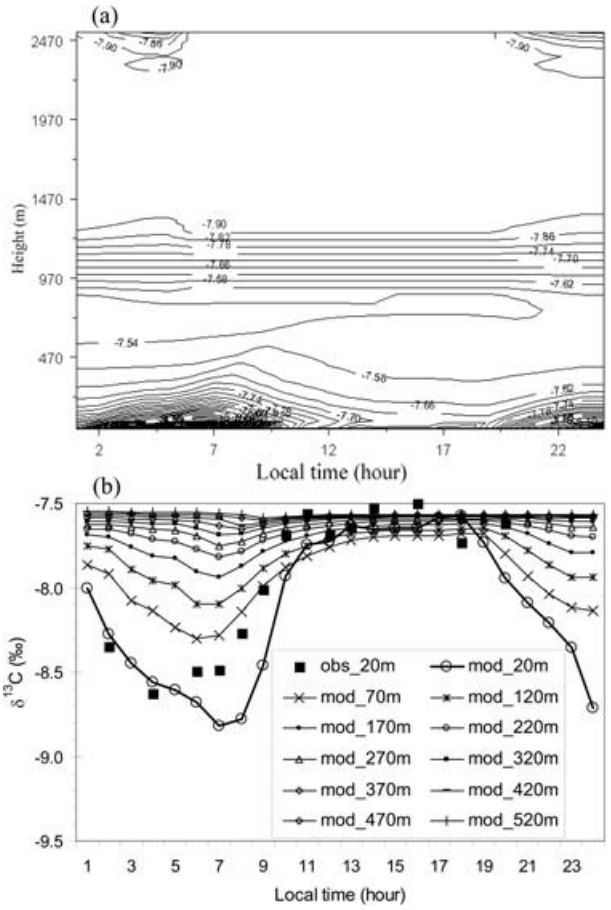

Fig. 2. Same as Fig. 1, but for 23 July 1999.

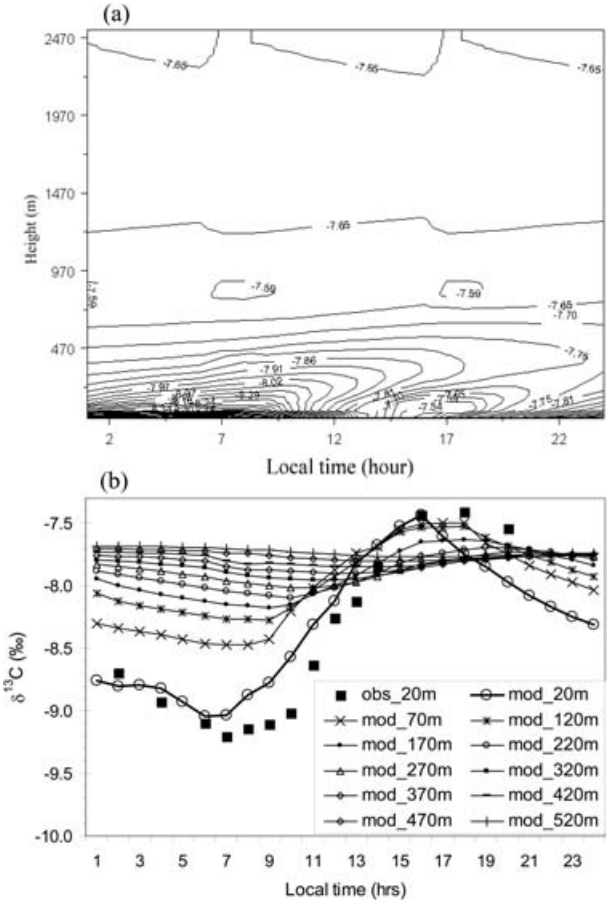

Fig. 3. Same as Fig. 1, but for 12 September 1999.

different phases of the growing season (Figs. 1–3). The day-to-day variability in the $\delta^{13}C$ vertical distribution of the diurnal cycle is a strong function of the characteristics (strength and thickness) of the PBL. Typically, a stable and shallow NBL will trap the nighttime respired CO_2 with depleted $^{13}CO_2$ near the surface and causes a large decline in $\delta^{13}C$. The decline reverses in the morning as the respiration gives way to photosynthesis and the surface inversion layer breaks down. Different intensities of radiative cooling and subsidence will result in strong inversion in a shallow layer with a corresponding large nocturnal decline in $\delta^{13}C$, or a weak inversion in a deep layer with a small nocturnal decline in $\delta^{13}C$. Different sensible heat fluxes and the change in potential temperature across the entrainment zone will lead to different mixing strength in the CBL with various vertical gradients in $\delta^{13}C$.

Simulated monthly composite diurnal cycles over a boreal forest region near FRD in August are shown in Fig. 4 as an example. Strong diurnal variations in $\delta^{13}C$ occurred near the surface layers, and the average magnitude of the diurnal cycle was dampened and time-lagged with increasing height. The modelled results illustrate again that the CO_2 diurnal vertical transport/mixing processes were modulated by diurnal variations in ecosystem respiration with depleted $^{13}CO_2$ at nighttime and enriched $^{13}CO_2$ during daytime due to photosynthetic discrimination, diurnal PBL dynamics, and the strength of the atmospheric nocturnal temperature inversion. The monthly composite diurnal amplitudes were greatest near the surface and decreased logarithmically with increasing height and were different from month to month (not shown). This decline was more pronounced during the growing season, as a consequence of the large magnitudes of both enriched $^{13}CO_2$ by photosynthetic discrimination and depleted $^{13}CO_2$ by respiration during the growing season.

3.2. Seasonal vertical profiles

Figure 5 shows simulated monthly averages of $\delta^{13}C$ of CO_2 at different heights from 20 to 2520 m above the ground, illustrating the seasonal cycles over the boreal region surrounding the FRD tower. $\delta^{13}C$ slightly varied in non-growing season months, followed by a gradual increase to June, then by a rapid increase up to annual maxima $\delta^{13}C$ values in August. A rapid decrease occurred through the fall at each level, reflecting a decrease in photosynthetic discrimination during the fall.

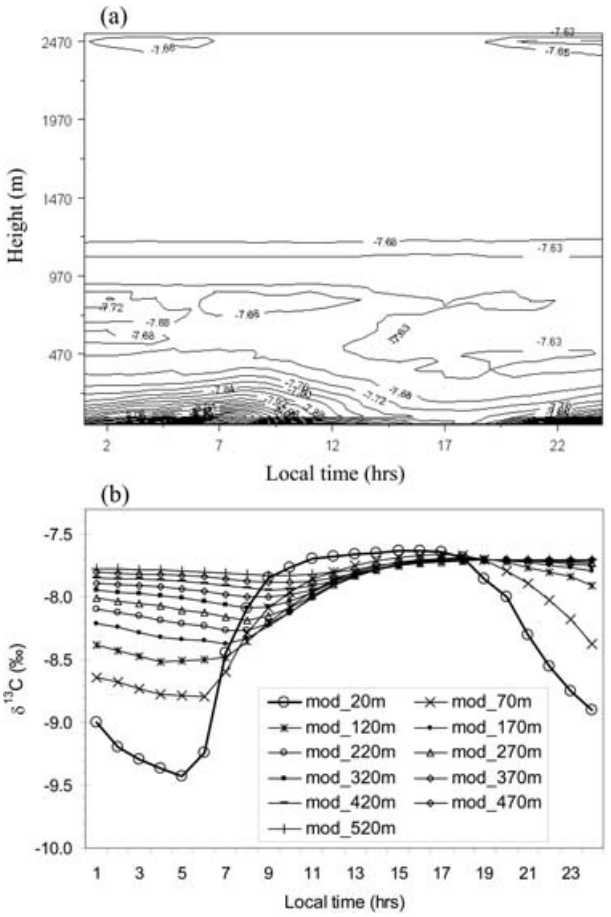

Fig. 4. Same as Fig. 1, but for monthly composite diurnal cycle of August 1999.

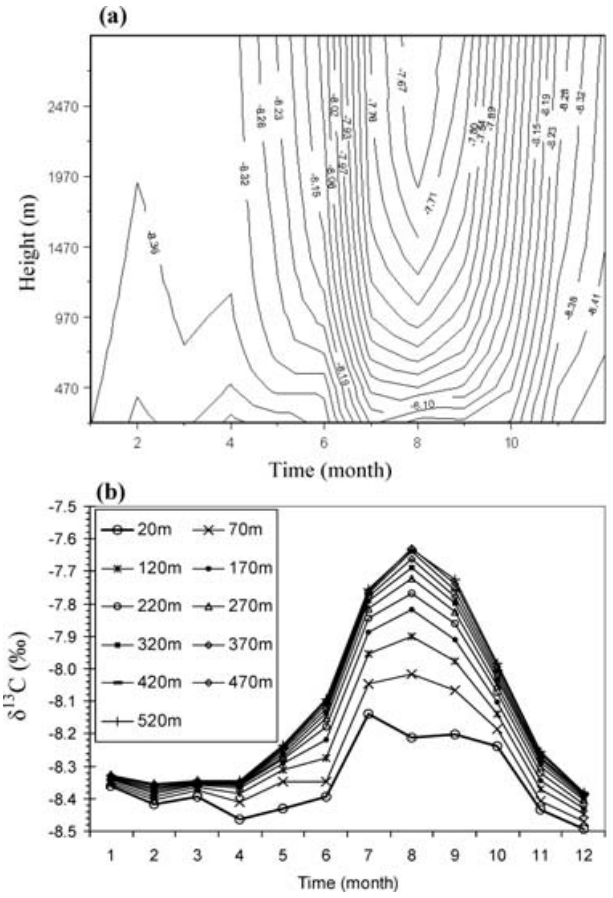

Fig. 5. Time–height cross-section of simulated monthly mean δ^{13}C of CO_2 in 1999. (a) Two-dimensional contour graph for δ^{13}C (unit: ‰) up to 2500 m; (b) simulated vertical profile of monthly mean δ^{13}C up to 520 m.

The modelled amplitudes of seasonal cycles of δ^{13}C increased with height from 0.35‰ at lower surface up to 0.7‰ at the top of model domain (Fig. 5a). There were large vertical gradients of δ^{13}C during the growing season with a maximum in August (around 0.6‰), while only 0.05–0.1‰ vertical differences during the non-growing season (November to April; Fig. 5), indicating the positive seasonal covariation between dynamics of the PBL and carbon isofluxes. Both uptake of carbon with high ratios of $^{12}CO_2$ by photosynthetic discrimination against $^{13}CO_2$ and release of carbon with high ratios of $^{12}CO_2$ by ecosystem respiration had large magnitudes during the growing season.

3.3. Does $\delta^{13}C$ imitate CO_2

The simulated monthly composite diurnal profile of CO_2 for August 1999 and seasonal profile of CO_2 for 1999 are also shown in Figs. 6 and 7, respectively. The simulated CO_2 concentrations at 20 m height followed tower measurements well at both diurnal and seasonal timescales with slight underestimations (Figs. 6 and 7), while their vertical patterns are consistent with the high tower observations (Bakwin et al., 1998). Comparing Fig. 6 with Fig. 4 and Fig. 7 with Fig. 5, the vertical patterns of δ^{13}C look like the mirror images of CO_2, but they are actually not, because the driving fluxes of CO_2 and δ^{13}C in the surface layer are not proportional.

The instantaneous carbon isotopic signature of net CO_2 flux ($\delta^{13}C_{bio}$) can be calculated using eqs. (1) and (2). As shown in Fig. 8, the differences between $\delta^{13}C_{bio}$and $\delta^{13}C_A$ and $\delta^{13}C_R$are significant. The potential difference between the CO_2 budget and the isotope tracer budget is considerable because of the different weighting factors of F_A and F_R (i.e. $\delta^{13}C_A$ and $\delta^{13}C_R$) and hence their vertical profiles (Figs. 4 and 5 for δ^{13}C; and Figs. 6 and 7 for CO_2). If we prescribe F_A and F_R to have the same CO_2 isotope signature, then there is

$$\delta^{13}C_A = \delta^{13}C_R = \overline{\delta^{13}C_{bio}} = \frac{F_{\delta 13,day}}{F_{net,C,day}}, \quad (3)$$

where $\overline{\delta^{13}C_{bio}}$ is daily overall carbon isotopic signature of net CO_2 flux, $F_{net,C,day}$ and $F_{\delta 13,day}$ are daily total net CO_2 flux and

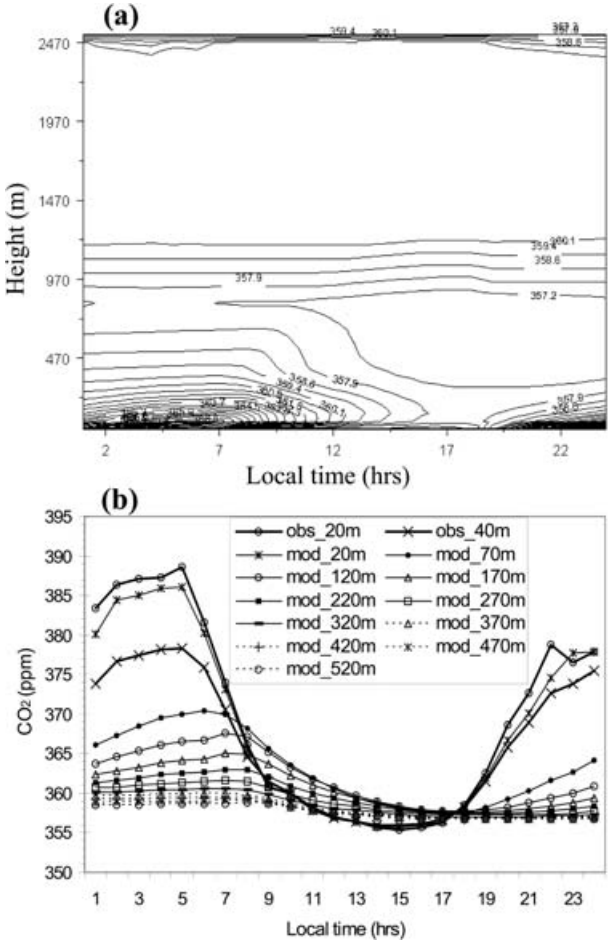

Fig. 6. Same as Fig. 1, but for monthly composite diurnal cycle of CO_2 for August 1999.

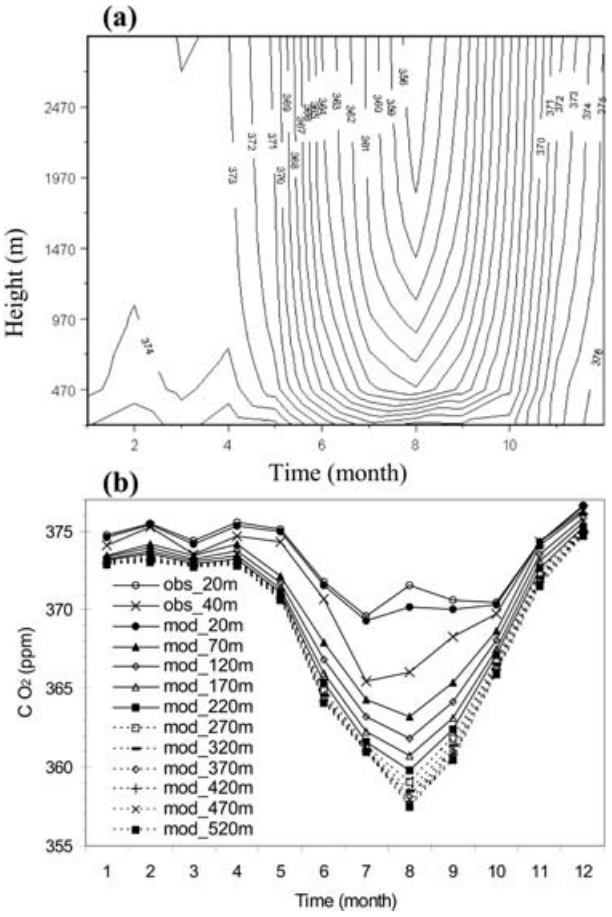

Fig. 7. Time–height cross-section of simulated monthly mean CO_2 in1999. (a) Two-dimensional contour graph (unit: ppm) up to 2520 m; (b) observed at 20 and 40 m height (obs˙20 m and obs˙40 m) and simulated monthly mean CO_2 from 20 to 520 m (mod˙20 ∼ mod˙520).

isoflux, respectively. Submitting eq. (3) in eq. (2), we can calculate a 'diagnostic' isoflux ($F_{\delta 13,\mathrm{equi}}$), which is a presumed isoflux under the condition that photosynthesis and respiration are confined to be in isotopic equilibrium.

As shown in Fig. 9, the monthly composite diurnal difference between the 'real' $F_{\delta 13}$ and the 'diagnostic' isoflux $F_{\delta 13,\mathrm{equi}}$ is considerable and the most difference occurred during the first 3–4 h of photosynthesis of a day.

To elucidate these differences or the expected extension information on $\delta^{13}C$ vertical profile to that of CO_2, we perform a model experiment. The VDS model is driven by $F_{\delta 13}$ and $F_{\delta 13,\mathrm{equi}}$ to simulate vertical patterns of $\delta^{13}C$ (refer to hereafter as model 1 and model 2, respectively). The simulated vertical profile of $\delta^{13}C$ by model 2 is expected to be a mirror image of CO_2, while that by model 1 inherently contains the disequilibrium isotopic fractionation effect. We assess the effect of the isotopic disequilibrium by ecosystem respiration and photosynthesis on vertical transport/mixing processes by comparing simulated vertical profiles of $\delta^{13}C$ with model 1 and model 2. Simulated diurnal and seasonal differences between model 1 and model 2 in vertical $\delta^{13}C$ profiles are shown in Figs. 10 and 11, respectively. Large differences between model 1 and model 2 in $\delta^{13}C$ were simulated near the surface layers and were dampened with increasing height on both diurnal and seasonal cycles. On diurnal cycle, the differences were much larger during nighttime than during daytime; similar to $\delta^{13}C$ vertical distribution, the differences between model 1 and model 2 was time-lagged with height. On seasonal timescale, the vertical profiles of $\delta^{13}C$ with model 1 and model 2 in non-growing season were identical, while the large difference was found in midgrowing season (June–August) with maximum in July.

Comparing Fig. 10 with Fig. 4b and Fig. 11 with Fig. 5b, we found that the difference in simulated vertical gradient between model 1 and model 2 was about 3–8%. The model results show that the vertical distribution of $\delta^{13}C$ absolutely differs from that of CO_2. It may be deduced that the isotopic disequilibrium effect

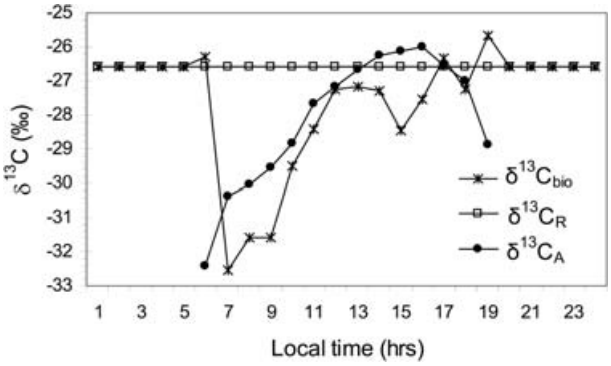

Fig. 8. Comparison of monthly composite diurnal variations in carbon isotopic signatures of net CO_2 flux ($\delta^{13}C_{bio}$), of gross primary production flux ($\delta^{13}C_A$), of ecosystem respiration flux ($\delta^{13}C_R$), for August 1999 in a boreal ecosystem near Fraserdale, Canada.

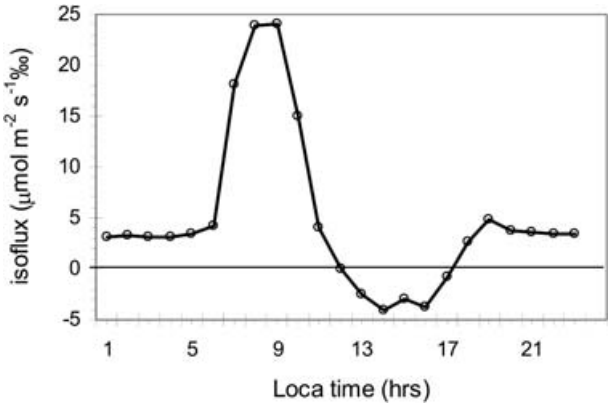

Fig. 9. Difference in monthly averaging of the diurnal cycle between 'real' isoflux $F_{\delta 13}$ by instantaneous $\delta^{13}C_{bio}$ and 'diagnostic' isoflux $F_{\delta 13,equi}$ by daily overall $\overline{\delta^{13}C_{bio}}$ for the August 1999 at FRD. The difference indicates the effect of isotopic disequilibrium between photosynthesis and respiration on isoflux.

on vertical distribution of $\delta^{13}C$ is considerable, especially in the surface layers.

4. Atmospheric rectification of carbon isotope

As discussed in Section 2, the terrestrial surface isofluxes represent both the diurnal oscillation and seasonal cycle. Similar to CO_2, the covariation between the terrestrial surface isofluxes and the atmospheric transport/convection through dynamics of the PBL on the diurnal, synoptic, and seasonal frequencies produces vertical and horizontal gradients of isotope signatures (i.e. $\delta^{13}C$). Analogue to atmospheric rectification of CO_2 (Keeling et al., 1989; Denning et al., 1995; Stephens et al., 2000), this covariation can be termed isotopic rectification. As the integrated VDS–BEPS-EASS isotope model has an overall capacity of simulating these processes well (Chen et al., 2004, 2005a,b), the model results could be useful in understanding the rectification

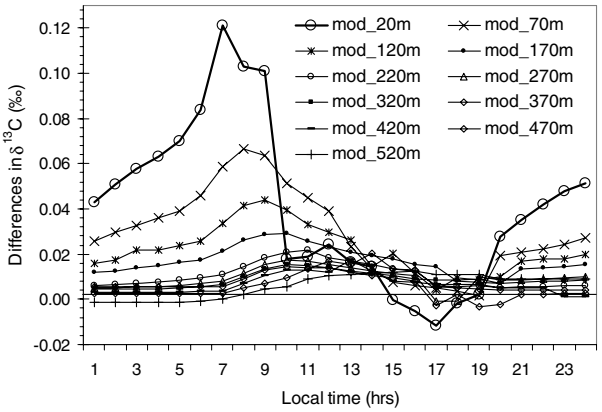

Fig. 10. Differences in simulated monthly composite diurnal cycles of $\delta^{13}C$ at different heights (20–520 m) between with isotopic disequilibrium (model 1) and without isotopic disequilibrium (model 2) for August 1999. The differences indicate the impact of isotopic disequilibrium between photosynthesis and respiration on vertical distribution of $\delta^{13}C$ of CO_2.

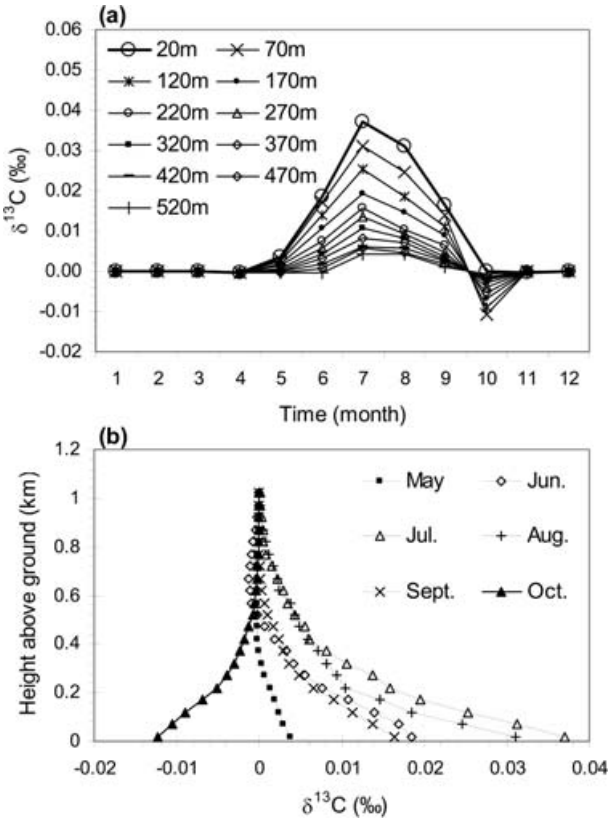

Fig. 11. Differences in simulated seasonal cycles of $\delta^{13}C$ at different heights between with isotopic disequilibrium (model 1) and without isotopic disequilibrium (model 2). (a) Differences in monthly mean $\delta^{13}C$ at different heights (20–520 m) for 1999; (b) vertical profiles (up to 1.2 km) of monthly mean difference for the growing season of 1999.

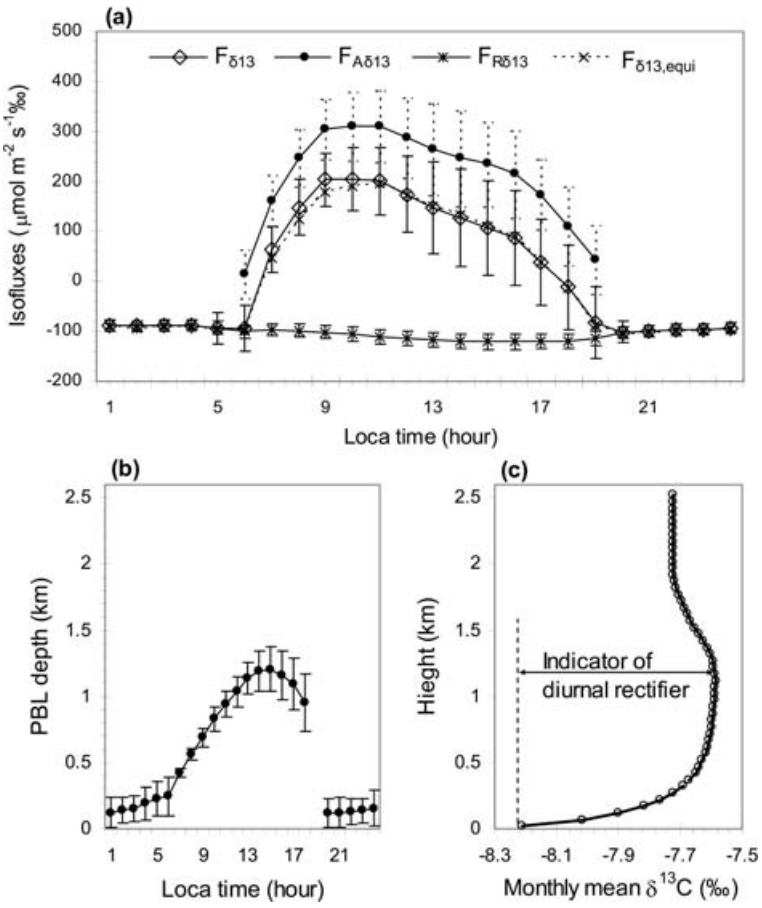

Fig. 12. Schematic showing the mechanism of the diurnal isotope rectification—an example from model simulations of August 1999, over a boreal region near Fraserdale, Ontario, Canada. (a) Simulated monthly composite diurnal isofluxes of δ^{13}C ($F_{\delta 13}$, $F_{A\delta 13}$, and $F_{R\delta 13}$), corresponding to net CO_2 flux (F_{net}), net assimilation (F_A), and total ecosystem respiration (F_R), respectively. The 'diagnostic' isoflux ($F_{\delta 13,equi}$) is also shown as comparison. (b) Simulated monthly composite diurnal dynamics of the PBL (z_i). And (c) a simulated vertical profile of monthly mean δ^{13}C of CO_2. The error bars in panels (a) and (b) indicate the standard deviation.

mechanism. The model presentation is divided into the diurnal and seasonal averages in order to differentiate the temporal scales that underpin the isotope rectifier effect.

4.1. Carbon isotope rectification by diurnal covariation

The monthly composite diurnal covariation during the growing season (e.g. August 1999) is shown in Fig. 12, along with the simultaneous surface isofluxes, PBL depth and the profile of δ^{13}C of CO_2. The diagnostic isoflux ($F'_{\delta 13,equi}$) is also shown. The most difference between $F'_{\delta 13}$ and $F_{\delta 13,equi}$ was found during early to middle morning. During the daytime in the growing season, photosynthetic uptake was much larger than ecosystem respirational release, and therefore the net isoflux to the atmosphere had a large positive value (up to 150 μmol m^{-2} s^{-1} ‰, Fig. 12a). The δ^{13}C enrichment process was associated with a deep convective PBL (Fig. 12b). This enriched δ^{13}C signal was weakened by strong dilution in the deep PBL. In contrast, the shallow stable NBL (Fig. 12b) trapped the CO_2 respired by ecosystem with depleted $^{13}CO_2$ near the surface (i.e. with negative net isoflux of around -100 μmol m^{-2} s^{-1} ‰, Fig. 12a). As a result of this diurnal covariation, the monthly mean δ^{13}C of CO_2 increases with height from the ground to the top of CBL (Fig. 12c).

The monthly mean vertical gradient in δ^{13}C can be considered as an indicator of the diurnal isotope rectification strength, which varies dramatically from season to season (Fig. 13). Diurnal isotope rectification is found to occur mostly during the growing season. The differences of simulated diurnal isotope rectifier effects between model 1 and model 2 are considerable during the growing season, which account for 5%, 6% and 8% for June, July and August, respectively (Fig. 13).

4.2. Carbon isotope rectification by seasonal covariation

The seasonal isotope rectification mechanism is schematically shown in Fig. 14 for 1999 as an example over the FRD tower area.

During the growing season (May to October), monthly mean $F_{A\delta 13}$ varied between around 2–10 mol m^{-2}d^{-1}‰ and the maxima occurred during June to August (Fig. 14a). The seasonal variation of F_R was significant with the maximum of about 9.5 mol m^{-2}d^{-1}‰ in July (Fig. 14a). The $F_{\delta 13}$ (the difference between $F_{A\delta 13}$ and $F_{R\delta 13}$) was still positive during the growing season months (i.e. net uptake of lighter^{12}C isotope by the ecosystem, leaving the air with relatively enriched with the heavier^{13}C isotope). The simulated monthly mean diagnostic isoflux ($F'_{\delta 13,equi}$) was lower than $F_{\delta 13}$ by 10–25% in growing season.

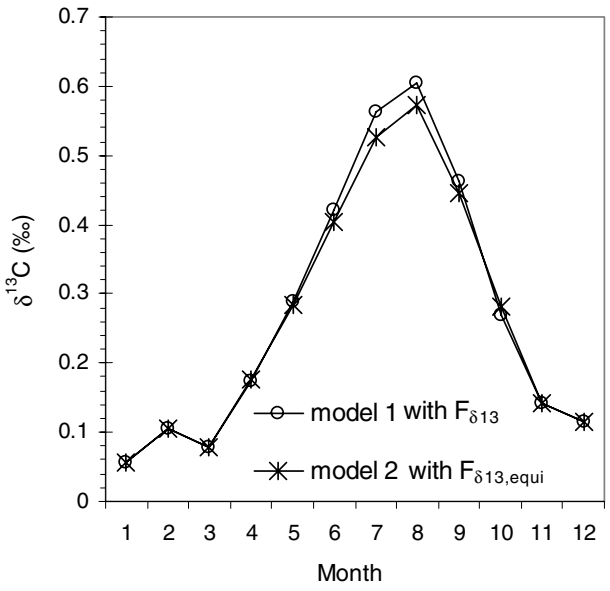

Fig. 13. Simulated monthly mean vertical difference in δ^{13}C between the top of CBL and the surface layer as an indicator of the isotope diurnal rectifier effect) in 1999, at Fraserdale, Ontario, Canada. The diurnal rectifier is found to be much stronger during the growing season than during the dormant season. And large difference between with isotopic disequilibrium (model 1) and without isotopic disequilibrium (model 2) in diurnal rectifier is simulated in the middle growing season. This difference accounts for 5%, 6% and 8% for June, July and August, respectively.

There was a small seasonal variation in the equilibrium NBL height, whereas the monthly averages of CBL depth was much lower during the dormant period of November through March than those during in the growing season. The CBL was the shallowest in midwinter (Fig. 14b) associated with a similar seasonal variation pattern of net isofluxes (Fig. 14a).

The seasonal covariation was characterized by deep mixing and large positive isofluxes (upwards) during the growing season and by shallow mixing and large respiration releases (negative isoflux) during the remaining period of the year. The enriched δ^{13}C signal by photosynthesis was diluted through deep mixing in the growing season, while the depleted δ^{13}C signal by respiration release was trapped near the surface in dormant season. In consequence, this seasonal covariation produced an annual mean vertical distribution with more negative δ^{13}C of CO_2 at the surface and less negative δ^{13}C aloft (Fig. 14c). In other words, the simulated annual mean vertical gradient of δ^{13}C would reflect the strength of the covariation between vertical transport and the surface isofluxes.

4.3. Partition of diurnal and seasonal carbon isotope rectifications

The covariation between the terrestrial surface isofluxes and the atmospheric transport or mixing at various timescales through diurnal, synoptic, and seasonal cycles leads to significant spatial gradients (both vertical and horizontal) in δ^{13}C of CO_2. This time-mean spatial gradient in the atmosphere is therefore a measure of the strength of this covariation (i.e. the magnitude of the isotope rectification).

When we performed a model experiment, in which the net carbon isoflux is prescribed without the diurnal cycle (e.g. using daily or monthly mean values and refer to hereafter as model 3), the diurnal and seasonal isotopic rectifier effects can be roughly extracted from the annual total (Fig. 15). The simulated annual mean vertical gradients of δ^{13}C using daily mean and monthly mean isofluxes are nearly identical. The simulated annual mean vertical gradient with model 3 should be mainly due to the seasonal isotopic rectifying effect, while the difference between model 1 and model 3 might come from rectifier effects at other intermediate timescales (e.g. synoptic and diurnal). The synoptic effect would be expected to be overall much weaker than the diurnal effect. The synoptic process can be not directly captured by a one-dimensional model (i.e. VDS), and therefore its rectification is not separated in this study. The annual mean gradient of δ^{13}C in the atmosphere from the surface layer (e.g. 20 m above the ground) to the annual mean seasonal maximum height of the CBL (around 1.2–1.4 km above the ground), quantified as the annual total atmospheric isotope rectifier effect, is simulated to be 0.248‰, 0.239‰ and 0.176‰ with model 1, 2 and 3, respectively, for 1999 over a boreal region in the vicinity of the FRD tower. The difference (around 3.5% of the total) between with model 1 and model 2 reflects the isotopic disequilibrium effect on rectification, while the difference (about 29% of the total) between with model 1 and model 3 indicates the diurnal rectifying effect. The model result also shows that the isotopic disequilibrium effect on δ^{13}C of CO_2 dynamics in PBL and the diurnal rectifying effect were confined to the surface layers (less than 350 m; Fig. 15B).

5. Conclusions

An ecosystem–boundary layer isotope model (VDS–BEPS-EASS) is employed to simulate dynamics of δ^{13}C of CO_2 in the PBL over a boreal forest region in the vicinity of the FRD tower in northern Ontario, Canada. The computed isotopic signatures (i.e. δ^{13}C values) in the surface layer during the growing season in 1999 agree well with intensive campaign data. We examine the interaction of the biosphere and the atmosphere with respect to δ^{13}C of CO_2, as well as the atmospheric mixing processes on diurnal and seasonal scales in 1999.

The covariation between the isotope fractionation/discrimination processes by ecosystem metabolism and atmospheric transport/mixing on various timescales (e.g. diurnal and seasonal) is reasonably well simulated, and the results are helpful to understand the carbon isotope rectification in atmospheric CO_2. Understanding the relationship between the carbon isotope rectification and the surface isofluxes will be

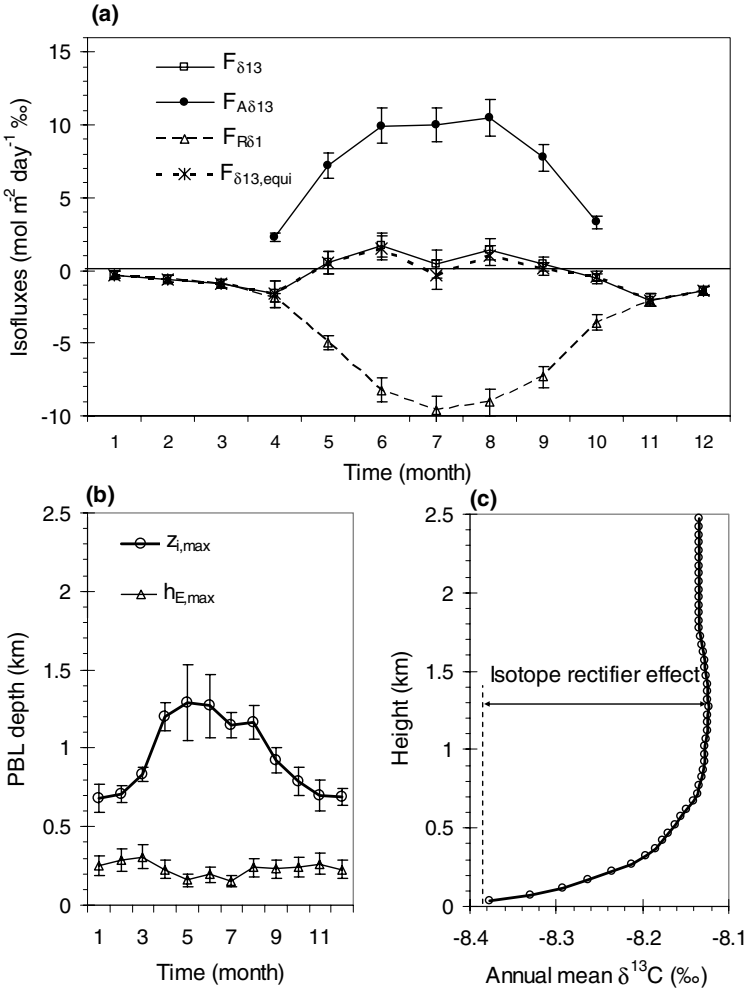

Fig. 14. Schematic showing the mechanism of the seasonal isotope rectification—an example from model simulations for 1999, over a boreal region near Fraserdale, Ontario, Canada. (a) Simulated seasonal variations in isofluxes of δ^{13}C: $F_{\delta 13}$, $F_{A\delta 13}$, and $F_{R\delta 13}$, corresponding to net CO_2 flux (F_{net}), net assimilation (F_A), and total ecosystem respiration (F_R), respectively. The simulated monthly mean "diagnostic" isoflux $F_{\delta 13,equi}$is also shown as comparison. (b) Simulated seasonal dynamics of the PBL: $z_{i,max}$ and $h_{E,max}$ are the monthly averages of daily maxima of the CBL depth and of the equilibrium height of NBL, respectively. And (c) a simulated vertical profile of annual mean δ^{13}C. The error bars in panels (a) and (b) indicate the standard deviation.

critically useful in using isotope data in atmospheric inversion for terrestrial carbon fluxes when the representativeness of isotope observations at fixed heights for the PBL is of concern. The model simulation illustrates that the diurnal vertical transport process of δ^{13}C is modulated by net isoflux with diurnal isotopic disequilibrium signature, diurnal PBL dynamics, and the strength of the atmospheric nocturnal temperature inversion; while the seasonal vertical distribution of δ^{13}C is characterized by deep mixing and large positive isoflux (upwards) during the growing season and by shallow mixing and large respirational releases (negative isoflux) during the remaining period of the year.

The simulated annual mean vertical gradient of δ^{13}C in the PBL, in terms of the isotopic rectifier effect, in the boreal region in vicinity of the FRD tower, was about 0.25‰ in 1999. The δ^{13}C gradient exhibited strong diurnal (29%) and seasonal (71%) variations that do not exactly mimic those of CO_2. Around 3.5% of the total gradient was contributed by isotopic disequilibrium of respiration and photosynthesis. This disequilibrium effect on δ^{13}C of CO_2 dynamics in PBL, moreover, was confined to the near surface layers (less than 350 m).

6. Acknowledgements

This work is supported by the Canadian Foundation for Climate and Atmospheric Sciences (project GC423). The technical contributions by D. Ernst and A. Chivulescu at MSC for the flask sampling and isotope measurements are appreciated. We would like to acknowledge Doug Worthy and M. Ernst (MSC) for the measurements of the CO_2 concentration and meteorology data at Fraserdale; B. Vaughan and J. White at INSTAAR, University of Colorado for isotope measurements of the flasks from MBL stations and K. Masarie at the NOAA/CMDL Carbon Cycle Group, for creating and updating the MBL reference fields. We also thank the two reviewers who made extensive comments/suggestions which are helpful to the paper revision.

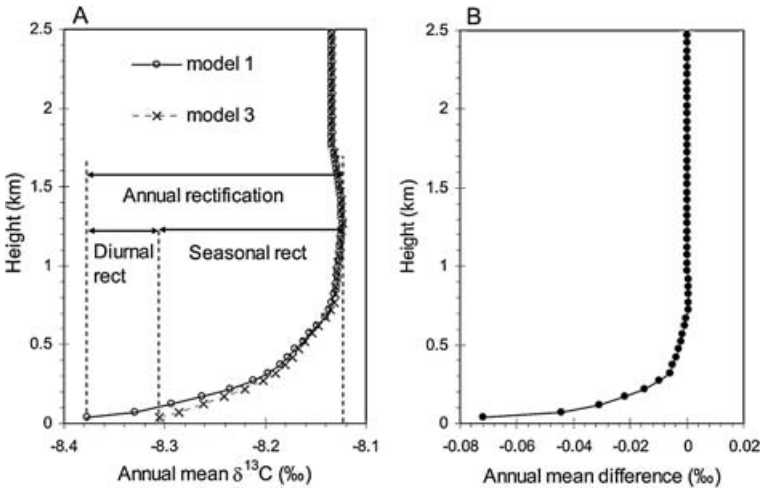

Fig. 15. Annual, seasonal and diurnal isotopic rectification. (A) Comparison of vertical patterns in annual mean $\delta^{13}C$ of CO_2 simulated by hourly (model 1) and daily (model 3) isofluxes from the ground to 2.5 km in 1999. (B) The effect of the diurnal cycle on the profile of simulated $\delta^{13}C$ (i.e. diurnal rectification), is seen as the difference between the hourly and daily calculations. Annual total isotope rectification (rect) is partitioned into diurnal and seasonal components.

References

Bakwin, P. S., Tans, P. P., White, J. W. C. and Andres, R. J. 1998. Determination of the isotopic ($^{13}C/^{12}C$) discrimination by terrestrial biology from a global network of observations. *Global Biogeochem Cycles*. **3**, 555–562.

Bristow, K. L. and Campbell, G. S. 1984. On the relationship between incoming solar radiation and daily maximum and minimum temperature. *Agric. For. Meteorol.* **31**, 159–166.

Chen, B., Chen, J. M., Liu, J., Chan, D., Higuchi, K. and co-authors.2004. A Vertical Diffusion Scheme to estimate the atmospheric rectifier effect. *J. Geophys. Res.* **109**, D04306, doi:10.1029/2003JD003925.

Chen, B., Chen, J. M. and Worthy, D. 2005a. Interannual variability in the atmospheric CO_2 rectification over a boreal forest region. *J. Geophys. Res.* **110**, D16301, doi:10.1029/2004JD005546.

Chen, B., Chen, J. M., Huang, L. and Tans, P. P. 2006. Modeling dynamics of stable carbon isotopic exchange between boreal ecosystems and the atmosphere. *Global Change Biol.* **12**, doi:10.1111/j.1365-2486.2006.01200.x.

Chen, J. M., Menges, C. H. and Leblanc, S. G. 2005b. Global mapping of foliage clumping index using multi-angular satellite data. *Remote Sens. Environ.* **97**, 447–457.

Chen, J. M., Pavlic, G., Brown, L., Cihlar, J., Leblanc, S. G. and co-authors. 2002. Validation of Canada-wide leaf area index maps using ground measurements and high and moderate resolution satellite imagery. *Remote Sens. Environ.* **80**, 165–184.

Ciais, P., Tans, P. P., White, J. W. C., Trolier, M., Francey, R. J. and co-authors. 1995a. Partitioning of ocean and land uptake of CO_2 as inferred by $\delta^{13}C$ measurements from NOAA Climate Monitoring and Diagnostics Laboratory Global Air Sampling Network. *J. Geophys. Res.* **100**(D3), 5051–5070.

Ciais, P., Tans, P. P., Trolier, M., White, J. W. C., Francey, R. J. 1995b. A large Northern Hemisphere terrestrial CO_2 sink indicated by the $^{13}C/^{12}C$ ratio of atmospheric CO_2. *Science* **269**, 1096–1101.

Cihlar, J., Beaubien, J., Latifovic, R. and Simard, G. 1999. Land cover of Canada 1995 Version 1.1. Digital data set documentation, Natural Resources Canada, Ottawa, Ontario. ftp://ftp2.ccrs.nrcan.gc.ca/ftp/ad/EMS/landcover95/.

Denning, A. S., Collatz, J. G., Zhang, C., Randall, D. A. Berry, J. A. and co-authors. 1996a. Simulations of terrestrial carbon metabolism and atmospheric CO_2 in a general circulation model. Part 1: Surface carbon fluxes. *Tellus* **48B**, 521–542.

Denning, A. S., Fung, I. Y. and Randall, A. D. 1995. Latitudinal gradient of atmospheric CO_2 due to seasonal exchange with land biota. *Nature* **376**, 240–243.

Denning, A. S., Randall, D. A., Collatz, G. J. and Sellers, P. J. 1996b. Simulations of terrestrial carbon metabolism and atmospheric CO_2 in a general circulation model. Part 2: spatial and temporal variations of atmospheric CO_2. *Tellus* **48B**, 543–567.

Denning, A. S., Takahashi, T. and Friedlingstein, P. 1999. Can a strong atmospheric CO_2 rectifier effect be reconciled with a "reasonable" carbon budget? *Tellus* **51B**, 249–253.

Enting, I. G., Trudinger, C. M. and Francey, R. J. 1995. A synthesis inversion of the concentration and $\delta^{13}C$ of atmospheric CO_2. *Tellus* **47B**, 35–52.

Fan, S., Gloor, M., Mahlman, J., Pacala, S., Sarmiento, J. and co-authors. 1998. A large terrestrial carbon sink in North America implied by atmospheric and oceanic carbon dioxide data and models. *Science* **282**, 442–446.

Farquhar, G. D. and Lloyd, J. 1993. Carbon and oxygen isotope effects in the exchange of carbon dioxide between terrestrial plants and the atmosphere. In: *Stable Isotopes and Plant Carbon-Water Relations*, (edsJ. R. Ehleringer, A. E. Hall and G. D. Farquhar). Academic, San Diego, CA, pp. 47–70.

Farquhar, G. D., Ehleringer, J. R. and Hubick, K. T. 1989. Carbon isotope discrimination and photosynthesis. *Ann. Rev. Plant Physiol. Plant Mol. Biol.* **40**, 503–537.

GLOBALVIEW-CO_2, 2005. Cooperative Atmospheric Data Integration Project: Carbon dioxide [CD-ROM]. NOAA Clim. Monit. and Diag. Lab., Boulder, Colo (Available via anonymous FTP to ftp.cmdl.noaa.gov, Path: ccg/co2/GLOBALVIEW).

Gurney, R. K., Law, R. M., Denning, A. S., Rayner, P. J., Baker, D. and co-authors. 2002. Towards robust regional estimates of CO_2 sources and sinks using atmospheric transport models. *Nature* **415**, 626–630.

Higuchi, K. and co-authors. 2003. Regional source/sink impact on the diurnal, seasonal and inter-annual variations in atmospheric

CO_2 at a boreal forest site in Canada. *Tellus* **55B**, 115–125.

Huang, L., Norman, A. L., Allison, C. E., Francey, R. J., Ernst, D. and co-authors. 2003. Traceability – maintenance for high precision stable isotope measurement ($\delta^{13}C$ & $\delta^{18}O$) of air-CO_2 by Lab-Carbonate-Standards at MSC: application to the Inter-Comparision Program (alert, Canada) with CSIRO, In: *The report to the 11th WMO/IAEA Meeting of Experts on CO_2 Concentration and Related Tracer Measurement Techniques*, Tokyo, Japan, Sept. 2001, No. 148, pp. 9–16.

Keeling, C. D., Bacastow, R. B., Carter, A. F., Piper, S. C., Whorf, T. P. and co-authors. 1989. A three-dimensional model of atmospheric CO_2 transport based on observed winds. I: analysis of observed data. In: Aspects of climate variability in the pacific and western americas (edited by D.H. Peterson, publisher: AGU, Washington, DC). *Geophys. Monogr.* **55**, 165–236.

Lacelle, B. 1998. Canada's soil organic carbon database. In: *Soil processes and the carbon cycle*, (edsR. Lal, J. Kimbla, R. F. Follett and B. A. Stewart). CRC Press, Boca Raton, 81–92.

Leblanc, S. G., Chen, J. M., White, H. P., Latifvic, R., Roujean, J. R. and co-authors. 2005. Canada-wide foliage clumping index mapping from multi-angular POLDER measurements. *Can. J. Remote Sens.* **31**, 364–376.

Lloyd, J. and co-authors. 1996. Vegetation effects on the isotopic composition of atmospheric CO_2 at local and regional scales: theoretical aspects and a comparison between rain forest in Amazonia and a boreal forest in Siberia. *Aust. J. Plant Physiol.* **23**, 371–399.

Masarie, K. A. and Tans, P. P. 1995. Extension and integration of atmospheric carbon dioxide data into a globally consistent measurement record. *J. Geophys. Res.* **100**(11), 593–1610.

Pearman, G. I. and Hyson, P. 1980. Activities of the global biosphere as reflected in atmospheric CO_2 records. *J. Geophys. Res.* **85**, 4468–4474.

Stephens, B. B. 1999. Field-based atmospheric O_2 measuremnets and the ocean carbon cycle. PhD Thesis. Scripps Institution of Oceanohraphy, La Jolla, California, 221 pp.

Stephens, B. B., Keeling, R. F., Tan, P. P., Heimann, M., Six, K. D., Murnane, R. and co-authors. 1998. Testing global ocean carbon cycle models using measurements of atmospheric O_2 and CO_2 concentration. *Global Biogeochem. Cycles* **12**, 213–230.

Stephens, B. B., Wofsy, S. C., Keeling, R. F., Tan, P. P. and Potosnak, M. J. 2000. The CO_2 budget and rectification airborne study: strategies for measuring rectifiers and regional. *Geophys. Monogr.* **14**, 311–324.

Tans, P. P. 1980. On calculating the transfer of carbon-13 in resevoir models of the carbon cycle. *Tellus* **32**, 464–469.

Tans, P. P., Berry, J. A. and Keeling, R. F. 1993. Oceanic $^{13}C/^{12}C$ observation: A new window on CO_2 uptake by the oceans. *Global Biogeochem. Cycles* **7**, 353–368.

Tarnocai, C., 1996. The amount of organic carbon in various soil orders and ecological provinces in Canada. In: *Soil Processes and the Carbon Cycle*, (edsR. Lal, J. Kimbla, R. F. Follett and B. A. Stewart). CRC Press, Boca Raton, FL, 81–92.

Winslow, J. C., Hunt, E. R. Jr and Piper, S. C. 2001. A globally applicable model of daily solar irradiance estimated from air temperature and precipitation data. *Ecol. Model.* **143**, 227–243.